SHAPE OPTIMIZATION OF ACOUSTIC BARRIERS BASED ON SUBDIVISION SURFACES BEM

CHUANG LU[1], LEILEI CHEN[2] & HAIBO CHEN[1]
[1] Department of Modern Mechanics, University of Science and Technology of China, CAS Key Laboratory of Mechanical Behavior and Design of Materials, P. R. China.
[2] College of Architecture and Civil Engineering, Xinyang Normal University, P. R. China.

ABSTRACT
This study presents a shape optimization approach for sound barrier using the isogeometric boundary element method based on subdivision surfaces. The geometry model is constructed through the subdivision scheme, and different control polygons/meshes describing the same curve/surface are used for geometry representation, boundary element analysis and optimization. The gradient-based optimization is implemented to minimize the sound pressure in the reference region. By subdivision coarsening treatment, the secondary processing improves the direct optimization results in reducing the oscillation of the optimized structure. The influence of different subdivision schemes on the obtained optimized configurations is studied in detail, which shows the potential of the secondary reverse processing for engineering prototype design.
Keywords: boundary element method, shape optimization, subdivision surfaces.

1 INTRODUCTION

As an effective and economical noise reduction tool, the sound barrier has been widely used in traffic noise control. The noise reduction effect of a sound barrier is related to the shape, size and material properties of the barrier [1, 2]. The optimization design of sound barrier can effectively improve its noise reduction effect. The isogeometric BEM based on NURBS has been applied to the structural optimization [3–5]. Subdivision surface can construct discontinuous discrete meshes of any topology into an overall smooth surface. In essence, a certain subdivision rule is used to repeat the subdivision processing of the polygonal mesh until the subdivision convergence limit is reached. At present, the optimization by means of subdivision surfaces is mainly applied to the distribution of sound absorbing materials [6], electrostatics [7] and elasticity problems [8]. This work aims to extend the shape optimization approach based on the subdivision surfaces BEM for sound barrier problems. We use fine control meshes for BEM discretisation and coarser control meshes for geometric modifications. The optimization is started from the coarsest initial control mesh, and the finer control meshes are gradually obtained. A key treatment of the present optimization approach is that a reverse processing is applied to the original optimized structure for reducing its oscillation.

2 SUBDIVISION ALGORITHM AND MULTIRESOLUTION

Constructing a subdivision curve requires a control polygon and a subdivision algorithm. A recursive refinement scheme is used to generate new polygons from the initial control polygon. The result of the limiting process is a smooth subdivision curve. The subdivision algorithm is a corner cutting scheme which can successively cut the corner with a fixed ratio.

Given an initial control polygon $(P_0^0, P_1^0, P_2^0, ..., P_n^0)$, for Chaikin algorithm shown in Fig. 1a, *i*th level of refinement on *j*th segment adopts the following equations:

ISSN: 2046-0546 (paper format), ISSN: 2046-0554 (online), http://www.witpress.com/journals
DOI: 10.2495/CMEM-V9-N2-108-116

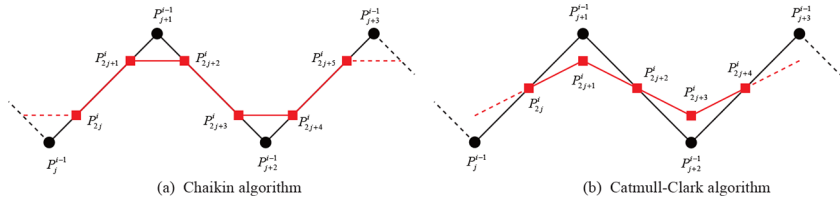

(a) Chaikin algorithm (b) Catmull-Clark algorithm

Figure 1: Computing new control points through the Chaikin and Catmull–Clark algorithms.

$$\begin{cases} P_{2j}^{i} = \dfrac{3}{4}P_{j}^{i-1} + \dfrac{1}{4}P_{j+1}^{i-1} \\ P_{2j+1}^{i} = \dfrac{1}{4}P_{j}^{i-1} + \dfrac{3}{4}P_{j+1}^{i-1} \end{cases} \tag{1}$$

For Catmull–Clark algorithm shown in Fig. 1b, *i*th level of refinement on *j*th segment adopts the following equations:

$$\begin{cases} P_{2j}^{i} = \dfrac{1}{2}P_{j}^{i-1} + \dfrac{1}{2}P_{j+1}^{i-1} \\ P_{2j+1}^{i} = \dfrac{1}{8}P_{j}^{i-1} + \dfrac{3}{4}P_{j+1}^{i-1} + \dfrac{1}{8}P_{j+2}^{i-1} \end{cases} \tag{2}$$

It has been shown that the limiting of a Chaikin curve is identical to a quadratic B-spline curve, while the Catmull–Clark curve converges to a cubic B-spline one. Figure 2 shows different levels of the subdivision curves from a concave polygon, obtained by the Chaikin and Catmull–Clark algorithms.

Here, we write the subdivision process as a linear mapping that maps a coarser control mesh at level l to a finer control mesh at level $l+1$

$$\mathbf{x}^{l+1} = \mathbf{A}\mathbf{x}^{l} \tag{3}$$

where $\mathbf{x}^{l}$ and $\mathbf{x}^{l+1}$ are two vectors containing the coordinates of all the vertices of the coarser and its refined polygons. $\mathbf{A}$ is the subdivision matrix and it contains the weights given by the

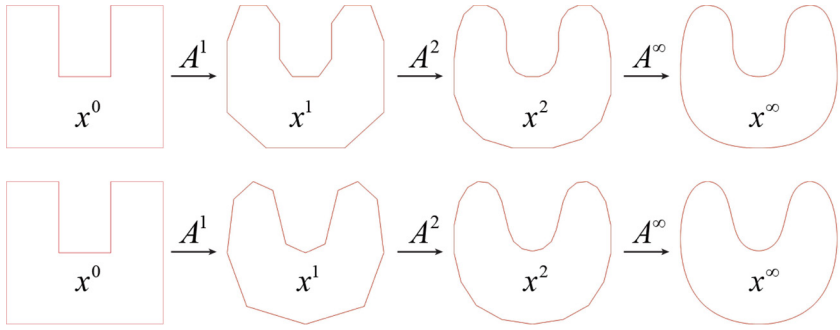

Figure 2: The concave polygons using two subdivision algorithms. The upper processing uses Chaikin algorithm, while the lower one applies the Catmull–Clark algorithm. The columns from left to right correspond to the initial control polygons, subdivision once, subdivision twice and the convergent curves, respectively.

subdivision stencils. The subdivision process can be interpreted as the chain of linear mappings for obtaining increasingly finer control meshes.

In this work, we introduce the coarsening of control meshes that are also obtained with subdivision. The linear coarsening matrix **B** maps the given control points at level $l+1$ to the control points at its coarser level l

$$\mathbf{x}^l = \mathbf{B}\mathbf{x}^{l+1} \tag{4}$$

The coarsening matrix **B** is formed by a least-squares fitting

$$\mathbf{x}^l = \underset{\mathbf{y}^l}{\operatorname{argmin}} \| \mathbf{x}^{l+1} - \mathbf{A}\mathbf{y}^l \|^2 \tag{5}$$

which leads to $\mathbf{A}^{\mathrm{T}}\mathbf{A}\mathbf{x}^l = \mathbf{A}^{\mathrm{T}}\mathbf{x}^{l+1}$. By comparing with eqn (4), **A** and **B** have the following relationship:

$$\mathbf{B} = (\mathbf{A}^{\mathrm{T}}\mathbf{A})^{-1}\mathbf{A}^{\mathrm{T}} \tag{6}$$

In words, one step of subdivision refinement of a given control mesh followed by coarsening does not change the nodal coordinates. The refinement and coarsening processes enable us to use different control meshes of the same geometry for optimization and analysis.

3 ACOUSTIC BEM AND SENSITIVITY ANALYSIS

For acoustic scattering problem, the total acoustic pressure is the sum of acoustic pressures caused by scattered acoustic wave and incident wave, i.e. $p(x) = p_{inc}(x) + p_{scat}(x)$. The Burton–Miller method that combines the conventional boundary integral equation and its normal derivative formulation overcomes the so-called fictitious eigenfrequency problem [3]. The two equations are as follows:

$$c(x)p(x) = \int_\Gamma \left[G(x,y)q(y) - F(x,y)p(y) \right] \mathrm{d}\Gamma + p_{inc}(x) \tag{7}$$

$$c(x)q(x) = \int_\Gamma \left[G^1(x,y)q(y) - F^1(x,y)p(y) \right] \mathrm{d}\Gamma + \frac{\partial p_{inc}(x)}{\partial n(x)} \tag{8}$$

where x is the source point, y is the field point, $q(y) = \partial p(y)/\partial n(y)$ and $n(y)$ denotes the outward normal vector at point y. The coefficient $c(x) = 1/2$ if the boundary Γ is smooth around the source point x. The kernel functions $G(x,y)$, $F(x,y)$, $G^1(x,y)$ and $F^1(x,y)$ can be found in [3]. In this study, the geometry can be expressed by B-spline curves as follows:

$$x(\xi) = \sum_{i=1}^{m_i} B_i(\xi) P_i \tag{9}$$

where m_i is the number of B-spline basis functions and P_i is the control point for the geometry. The quadratic and cubic B-spline basis functions can be expressed as

$$B_1(\xi) = \frac{1}{2}(\xi^2 - 2\xi + 1), \quad B_2(\xi) = \frac{1}{2}(-2\xi^2 + 2\xi + 1), \quad B_3(\xi) = \frac{1}{2}\xi^2 \tag{10}$$

$$B_1(\xi) = \frac{1}{6}(-\xi^3 + 3\xi^2 - 3\xi + 1), \quad B_2(\xi) = \frac{1}{6}(3\xi^3 - 6\xi^2 + 4),$$

$$B_3(\xi) = \frac{1}{6}(-3\xi^3 + 3\xi^2 + 3\xi + 1), \quad B_4(\xi) = \frac{1}{6}\xi^3 \tag{11}$$

Similarly, the sound pressure and flux at the boundary are interpolated using B-spline basis functions as follows:

$$p(\xi) = \sum_{i=1}^{m_i} B_i(\xi) p_i, \qquad q(\xi) = \sum_{i=1}^{m_i} B_i(\xi) q_i \tag{12}$$

where p_i and q_i represent the nodal parameters associated with the sound pressure and normal flux, respectively. The Burton–Miller formulation can be discretized in matrix form as:

$$\mathbf{Hp} = \mathbf{Gq} + \mathbf{p_i} \tag{13}$$

Acoustic sensitivity analysis is a critical step in the shape optimization of acoustic structures. Using the direct differentiation method, the equations are given as

$$\begin{aligned} c(x)\dot{p}(x) = & \int_\Gamma [\dot{G}(x,y)q(y) - \dot{F}(x,y)p(y)]\mathrm{d}\Gamma(y) \\ & + \int_\Gamma [G(x,y)\dot{q}(y) - F(x,y)\dot{p}(y)]\mathrm{d}\Gamma(y) \\ & + \int_\Gamma [G(x,y)q(y) - F(x,y)p(y)]\mathrm{d}\dot{\Gamma}(y) + \dot{p}_{inc}(x) \end{aligned} \tag{14}$$

$$\begin{aligned} c(x)\dot{q}(x) = & \int_\Gamma [\dot{G}^1(x,y)q(y) - \dot{F}^1(x,y)p(y)]\mathrm{d}\Gamma(y) \\ & + \int_\Gamma [G^1(x,y)\dot{q}(y) - F^1(x,y)\dot{p}(y)]\mathrm{d}\Gamma(y) \\ & + \int_\Gamma [G^1(x,y)q(y) - F^1(x,y)p(y)]\mathrm{d}\dot{\Gamma}(y) + \frac{\partial \dot{p}_{inc}(x)}{\partial n(x)} \end{aligned} \tag{15}$$

where the upper dot $(\dot{})$ denotes the differentiation with respect to the design variable. The shape sensitivities of sound pressure and its flux are interpolated from their respective nodal values

$$\dot{p}(\xi) = \sum_{i=0}^{m_i} B_i(\xi)\dot{p}_i, \qquad \dot{q}(\xi) = \sum_{i=0}^{m_i} B_i(\xi)\dot{q}_i \tag{16}$$

Here, the matrix form of the combined Burton–Miller formulation of eqns (14) and (15) can be expressed as

$$\dot{\mathbf{H}}\mathbf{p} + \mathbf{H}\dot{\mathbf{p}} = \dot{\mathbf{G}}\mathbf{q} + \mathbf{G}\dot{\mathbf{q}} + \dot{\mathbf{p}}_\mathbf{i} \tag{17}$$

where $\dot{\mathbf{H}}$ and $\dot{\mathbf{G}}$ are the corresponding sensitivity coefficient matrices and $\dot{\mathbf{p}}$ and $\dot{\mathbf{q}}$ are the sensitivities of $\mathbf{p}$ and $\mathbf{q}$.

4 SHAPE OPTIMIZATION

The acoustic shape optimization problem can be formulated as

$$\begin{cases} \min & \Pi = \bar{\mathbf{p}}_f \mathbf{p}_f \\ \text{s.t.} & A \le A_0 \\ & x_i^l \le x_i \le x_i^u \end{cases} \tag{18}$$

where $\mathbf{p}_f$ is the sound pressure vector at the reference point x_f and $\bar{\mathbf{p}}_f$ denotes its complex conjugate. In this work, the coordinates of control points are set as design variables. Π is the objective function. The optimization constraint is the designed area A smaller than the initial area A_0, and x_i^l and x_i^u represent the lower and upper limits of the design variables, respectively.

The sensitivity of the objective function to the design variable can be expressed as

$$\frac{\partial \Pi}{\partial x_i} = \frac{\partial (\bar{\mathbf{p}}_f \mathbf{p}_f)}{\partial x_i} = 2\Re(\bar{\mathbf{p}}_f \mathbf{p}_f) \tag{19}$$

where Π is the real part of the complex number. The expression for the sound pressure vector $\mathbf{p}_f$ in the acoustic domain can be calculated by the discretized formulation:

$$\mathbf{p}_f = -\mathbf{H}\mathbf{p} + \mathbf{G}\mathbf{q} + \mathbf{p}_\mathbf{i} \tag{20}$$

By differentiating $\mathbf{p}_f$ with respect to design variable x_i, the following formulation can be obtained:

$$\mathbf{p}_f = -\dot{\mathbf{H}}\mathbf{p} - \mathbf{H}\dot{\mathbf{p}} + \dot{\mathbf{G}}\mathbf{q} + \mathbf{G}\dot{\mathbf{q}} + \dot{\mathbf{p}}_\mathbf{i} \tag{21}$$

Here, we employ the method of moving asymptotes (MMA) as the optimizer to update the design variables as shown below:

$$\frac{\left|\Pi^{t+1} - \Pi^t\right|}{\Pi^t} < \tau \tag{22}$$

where t denotes the iteration step and Π^t represents the value of objective function at t th iteration. τ is the iterative convergence criterion, set as 1.0×10^{-4}.

5 NUMERICAL TESTS

To demonstrate the validity and applicability of the developed optimization algorithm, we consider the analysis and design domain of a vertical noise barrier shown in Fig. 3. The thickness of the barrier is set as 0.25 m and a monopole source is located at $(0,1)m$. As the figure shows, the left vertical boundary of the noise barrier is selected as the line to be optimized. The design variables are the horizontal coordinates of the N control points of the designing vertical line, and the optimization objective is to minimize the mean sound pressure on the reference plane.

The acoustic scattering of the sound barrier is a half-space problem, and the kernel function can be written as

$$G(x,y) = \frac{i}{4} H_0^{(1)}(kr) + \frac{i}{4} H_0^{(1)}(kr' \tag{23}$$

where $r' = |x' - y|$ and x' is the mirror point of the source point x. Make the same changes to other kernel functions in the above formulations. After obtaining the basic sound pressure and sensitivity information, use the MMA solver to iterate the design variables until the iteration convergence accuracy is satisfied.

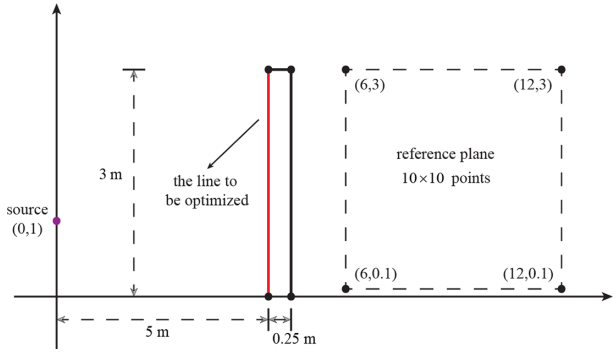

Figure 3: Initial sound barrier.

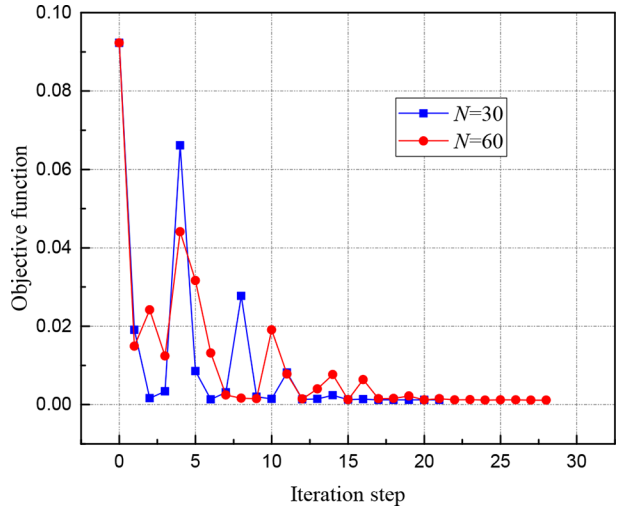

Figure 4: Objective function with iteration step for numbers of inserting control points 30 and 60; the computing frequency is 300 Hz.

Figure 4 shows the objective function varying with the iteration step for different numbers of control points. Obviously, with an increase in design variables, the number of iteration steps also tends to increase. A larger N produces a smaller optimal value of the objective function, where the convergent value is 0.00122 when $N = 30$ and 0.00117 when $N = 60$. Figures 5 and 6 show the shape configurations of the sound barrier at different control points N with frequency 300 Hz. Adding geometric control points can improve the flexibility in shape optimization, and we can find that the oscillation of the optimization line increases obviously. In order to eliminate this feature, the reverse matrix processing method is used to reduce the local oscillation of the optimized boundary. Figure 7 shows the detailed optimization process in Fig. 6. After the directly optimized Chaikin curve 1 is obtained, the boundary consisting of control points is coarsened once through the coarsening matrix, so as to obtain the boundary of the third subgraph shown in Fig. 7, and finally it is subdivided into a Chaikin curve 2 to meet the design requirements of the structure.

The sensitivity distributions of the control points at different frequencies are different, and the corresponding optimization results are also different. Now the number of geometric

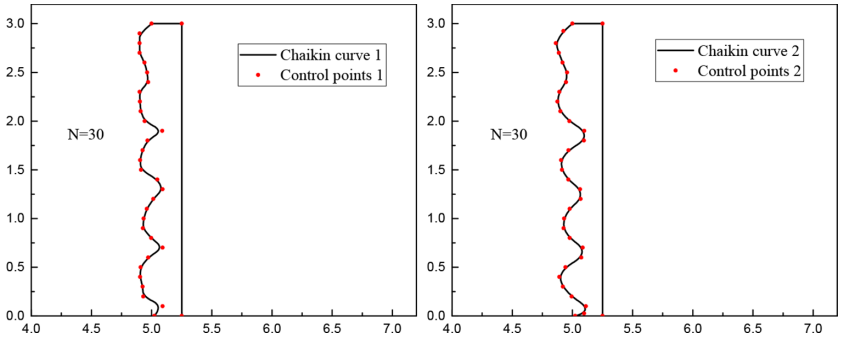

Figure 5: Final optimal solution and coarsening matrix processing solution for $N = 30$ with frequency 300 Hz.

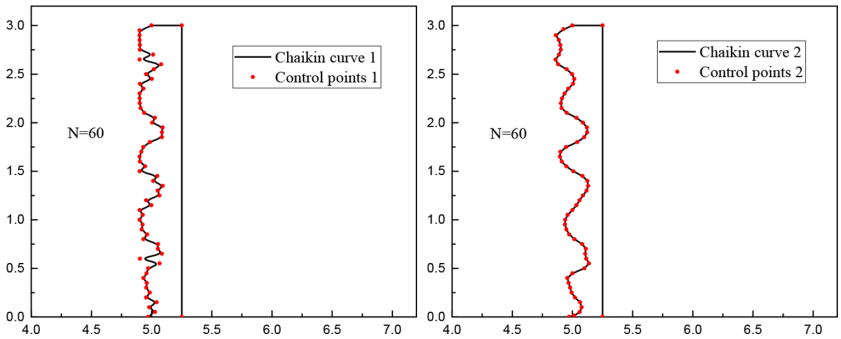

Figure 6: Final optimal solution and coarsening matrix processing solution for $N = 60$ with frequency 300 Hz.

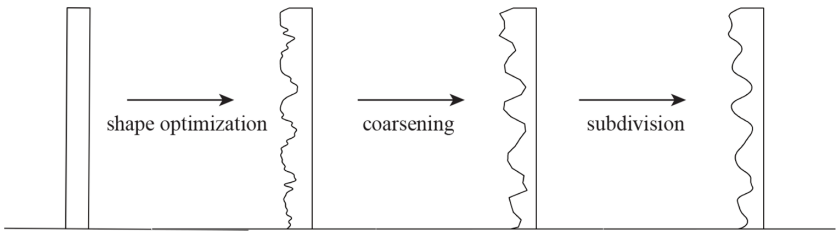

Figure 7: Optimize the initial sound barrier and reverse processing operation to obtain a reasonable structure.

control points is fixed at $N = 60$. Figures 8 and 6 show the final shapes of the sound barrier after optimization at 150 and 300 Hz, respectively. For the optimized boundary, more peaks and valleys are found in higher frequencies. Table 1 shows the comparison of the noise reduction effect before and after optimization. The *optimization value* 1 represents the result of the direct optimization of the initial sound barrier, and the *optimization value* 2 represents the optimization result obtained through the inverse matrix processing. It can be found that the two optimized results are basically the same, indicating that the method is feasible and effective.

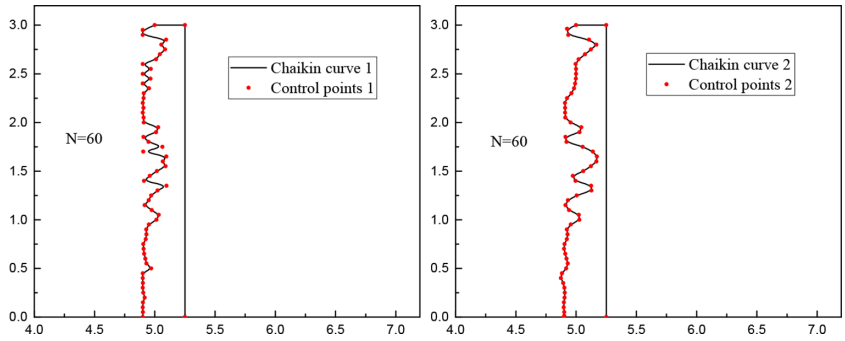

Figure 8: Final optimal solution and coarsening matrix processing solution with frequency 150 Hz.

Table 1: Comparison of average sound pressure levels before and after optimization at different frequencies for the test points in the reference plane.

Frequency	**Initial value**	**Optimization value 1**	**Optimization value 2**
Hz	**dB**	**dB**	**dB**
150	43.8676	38.2236	38.4284
300	46.8073	41.7451	41.9468

6 CONCLUSIONS

A shape optimization approach based on subdivision surfaces is proposed for the sound barrier in this work. Numerical tests show the validity of the proposed approach and the necessity of an optimal design. The optimal noise reduction structure is obtained through the refinement of the optimization results and the reverse operation processing, which provides a set of reasonable solutions for the production and design structure.

ACKNOWLEDGMENTS

This work is financially supported by the National Natural Science Foundation of China (NSFC) under Grant Nos 11772322 and 11872168 and the Strategic Priority Research Program of the Chinese Academy of Sciences under Grant No. XDB22040502.

REFERENCES

[1] Ishizuka, T. & Fujiwara, K., Performance of noise barriers with various edge shapes and acoustical conditions. *Applied Acoustics*, **65**, pp. 125–141, 2004. https://doi.org/10.1016/j.apacoust.2003.08.006

[2] Monazzam, M. & Lam, Y., Performance of profiled single noise barriers covered with quadratic residue diffusers. *Applied Acoustics*, **66**, pp. 709–30, 2005. https://doi.org/10.1016/j.apacoust.2004.08.008

[3] Liu, C., Chen, L. & Zhao, W., Chen H. Shape optimization of sound barrier using an isogeometric fast multipole boundary element method in two dimensions. *Engineering Analysis with Boundary Elements*, **85**, pp. 142–157, 2017. https://doi.org/10.1016/j.enganabound.2017.09.009

[4] Chen, L., Liu, C., Zhao, W. & Liu, L., An isogeometric approach of two dimensional acoustic design sensitivity analysis and topology optimization analysis for absorbing material distribution. *Computer Methods in Applied Mechanics and Engineering*, **336**, pp. 507–532, 2018. https://doi.org/10.1016/j.cma.2018.03.025

[5] Chen, L., Lian, H., Liu, Z. & Chen, H., Atroshchenko, E. & Bordas, S.P.A., Structural shape optimization of three dimensional acoustic problems with isogeometric boundary element methods. *Computer Methods in Applied Mechanics and Engineering*, **335**, pp. 926–951, 2019. https://doi.org/10.1016/j.cma.2019.06.012

[6] Chen, L., Lu, C., Lian, H., Liu, Z., Zhao, W., Li, S., Chen, H. & Bordas, S.P.A., Acoustic topology optimization of sound absorbing materials directly from subdivision surfaces with isogeometric boundary element methods. *Computer Methods in Applied Mechanics and Engineering*, **362**, 112806, 2020. https://doi.org/10.1016/j.cma.2019.112806

[7] Bandara, K., Cirak, F., Of, G., Steinbach, O. & Zapletal, J., Boundary element based multiresolution shape optimisation in electrostatics. *Journal of Computational Physics*, **297**, pp. 584–598, 2015. https://doi.org/10.1016/j.jcp.2015.05.017

[8] Bandara, K., Rueberg, T. & Cirak, F., Shape optimisation with multiresolution subdivision surfaces and immersed finite elements. *Computer Methods in Applied Mechanics and Engineering*, **300**, pp. 510–539, 2016. https://doi.org/10.1016/j.cma.2015.11.015